

Multistatic Radar Low Probability of Intercept signaling for the enhancement of target detectability in an adverse electromagnetic environment

Th. Papastamatis^a, K. Ioannou^b, I. Koukos^c and T. Xenos^e

^a *Hellenic Air Force, Lieutenant, Ph.D. Candidate, Aristotle University of Thessaloniki, Greece*

^b *Hellenic Navy, Lieutenant Junior Grade, PhD Candidate, Aristotle University of Thessaloniki, Greece*

^c *Combat Systems Sector, Hellenic Naval Academy, Piraeus, Greece*

^d *Aristotle University of Thessaloniki, Greece*

Abstract. Low Probability of Intercept (LPI) waveforms have been used so far in monostatic radar signaling for pulse compression that results in drastic improvement of radar resolution or granularity. Multistatic radar becomes increasingly important due to its alleged ability to detect stealth aircraft. However opportunistic exploitation of TV, FM radio or GSM Cellular emissions will not safeguard acceptable probability of detection levels, therefore the design of special signals emitted from dedicated beacons is a way to bring out all stealth's design weaknesses. This paper analyzes LPI waveforms via their Autocorrelation, their Periodic Ambiguity and Periodic Autocorrelation Functions for the bistatic radar which will open the way to discover new optimum target detection geometries and denoising strategies.

Keywords. -Low Probability of Intercept, Ambiguity Functions, Autocorrelation Functions, Bistatic Radar

1. INTRODUCTION

Airwaves are awash with commercial radiowave broadcasts emitted by WiFi, WiMax transmissions, DVB TV, FM radio or GSM *cellular phone* stations. Military researchers have thought long ago of using them as sources of RF radiation as a substitute of radar transmitters. This freely available radiation reflected from flying objects of any kind, will form a multistatic opportunistic passive radar that will detect a target by generating position and kinematic tracks equivalent to those of a regular monostatic radar. Furthermore, stealthy targets will be detected with much higher probability because a multistatic radar receiver can catch scattered reflections from a stealth aircraft which is structurally optimized only to minimize reflected signal from the direction of the illuminating source and cannot prevent scattering of radiation to other directions.

A radar detector classically searches the trace of a target in the output of a matched filter. Classically, the performance of a radar waveform is evaluated and presented in terms of the ambiguity function, originated in the 1950s by F. Gini et. al. [1], and which expresses the point

target response of the signal $u(t)$ as a function of delay τ and Doppler shift ν (or equivalently target range and velocity),

$$|\chi(\tau, \nu)|^2 = \left| \int u(x) u^*(x + \tau) \exp(j2\pi\nu x) dx \right|^2 \quad (1)$$

in the form of two dimensional plot.

2. THE BISTATIC RADAR EQUATION

The range equation for a monostatic radar is given by [2] :

$$R = \left[\frac{P_T G_T G_R \lambda^2 \sigma F^4}{(4\pi)^3 k T_s B_n (S/N)_{\min} L} \right]^{1/4} \quad (2)$$

where R is the range from the radar to the target, P_T is the transmitter power output, G_T is the transmitting antenna gain, G_R is receiving antenna gain, λ is the carrier wavelength, σ is target cross section, F is the atmospheric attenuation factor, k is Boltzmann's constant, T_s is receiving system noise temperature, and B_n is the receiver's noise bandwidth, $(S/N)_{\min}$ is the minimum SNR required for detection, and L accounts for various losses. The coverage area resembles a circle around the radar. This causes the SNR to be constant at a given range [2]:

$$(S/N) = \left[\frac{P_T G_T G_R \lambda^2 \sigma F^4}{(4\pi)^3 k T_s B_n L R^4} \right] \quad (3)$$

The lines of constant SNR around the node are called SNR contours stemming from the geometric Cassini curve. The circular shape of the SNR contours means that the area is calculate by [6]:

$$A = \pi R^2$$

where R is the distance from the node to a given Cassini curve.

For the bistatic radar, the maximum range equation is given by [2] :

$$(R_T R_R)_{\max} = \left[\frac{P_T G_T G_R \lambda^2 \sigma F_T^2 F_R^2}{(4\pi)^3 k T_s B_n (S/N)_{\min} L} \right]^{1/2} = \kappa \quad (4)$$

where R_T is transmitter to target range, R_R is receiver to target range, F_T is the atmospheric attenuation factor from the transmitter to the target, F_R is the atmospheric attenuation factor from the target to the receiver, and κ is the bistatic maximum range product.

Each Cassini oval represents a constant SNR level. R_T and R_R change as their intersection on a given SNR contour moves. The target position is considered to be this point of intersection. From the above equation, the SNR of the bistatic radar is given by [2] :

$$(S/N) = \left[\frac{P_T G_T G_R \lambda^2 \sigma F_T^2 F_R^2}{(4\pi)^3 k T_s B_n L R_T^2 R_R^2} \right] \quad (5)$$

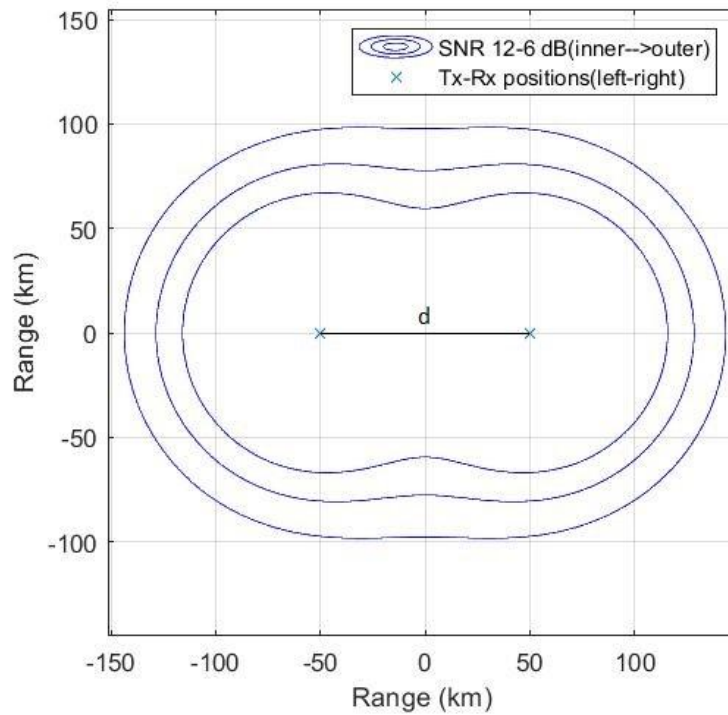


Figure 1. Bistatic radar Cassini ovals

From [2] we can also derive the area within the ovals of Cassini for a bistatic system, which can be used to compare different bistatic systems. This area is given as [2]:

$$A_B \approx \pi\kappa \left[1 - \left(\frac{1}{2}\right)^2 \left(\frac{d^4}{16\kappa^2}\right) \left(\frac{1}{1}\right) - \left(\frac{1*3}{2*4}\right)^2 \left(\frac{d^4}{16\kappa^2}\right)^2 \left(\frac{1}{3}\right) - \dots \right] \approx \pi\kappa \left[1 - \left(\frac{d^4}{64\kappa^2}\right) - \left(\frac{3d^8}{16384\kappa^4}\right) \right] \quad (6)$$

3. NETTED RADAR

The netted radar system is a network of identical systems at each node, using the synchronization across transmitters and receivers. The target is an isotropic scatterer and a noise limited system performance has been achieved. Such a distributed radar system allows the potential SNR gains to approach n^2 where n is the number of sensor nodes. Synchronization is the key requirement in order to realize this potential.

The general radar range equation is modified to yield the range equation for the distributed radar [2]:

$$(S / N) = \sum_{i=1}^n \sum_{j=1}^n \left[\frac{P_T G_T G_R \lambda^2 \sigma F_T^2 F_R^2}{(4\pi)^3 k T_s B_n L R_{Ti}^2 R_{Rj}^2} \right] = \sum_{i=1}^n \sum_{j=1}^n (S / N)_{ij} \quad (7)$$

where R_{Ti} is range from transmitter i to the target, R_{Rj} is range from receiver j to the target, and $(S/N)_{ij}$ is the SNR when node i is the transmitter and j is the receiver. The indices of summation are due to the collective nature of the system as every node transmits a pulse and all radars receive returns due to every transmitted pulse. Each of these actions contributes to the overall system's SNR, resulting in the potential n^2 gains. Table 1 illustrates the affect the indices of summation have on the total SNR for a distributed radar network with $n=3$. The rows represent the summation over i and the columns represent the summation over j .

	j=1	j=2	j=3
i=1	T_{X1}/R_{X1}	T_{X1}/R_{X2}	T_{X1}/R_{X3}
i=2	T_{X2}/R_{X1}	T_{X2}/R_{X2}	T_{X2}/R_{X3}
i=3	T_{X3}/R_{X1}	T_{X3}/R_{X2}	T_{X3}/R_{X3}

Table 1. Distributed radar network

In order to evaluate the performance of radar systems with different numbers of nodes, a means to plot these systems must be developed. This section expands the work done in [4] in order to develop a means to compare a monostatic radar system to a distributed radar system.

i. GENERAL EXPRESSION FOR R

The Cassini curve is a curve for which the product of multiple polar radii is constant. This is a generalization of the definition of Cassini oval ($n = 2$) provided in [2], as described above. This definition is expressed as [2]:

$$\prod_{i=1}^n R_i = a \quad (8)$$

where n is the number of nodes R_i is the distance from the i th node to a Cassini curve and α is a constant. The general equation for R , which is the distance from the origin point on a Cassini curve (given in polar form), is [2]:

$$R^n = 2 \cos n\theta + \frac{\alpha - 1}{R^n} \quad (9)$$

where θ is the angle used in the polar plot ($0 \leq \theta \leq 2\pi$). Manipulating terms in the above equation yields the range from the origin to a point on a Cassini curve [2]:

$$R = r^n \sqrt{\cos n\theta \pm \sqrt{\alpha - \sin^2 n\theta}} \quad (10)$$

where r is the radius from the origin to each node (and therefore dictates the size of the curves).

The geometry of the sensor network affects the variable r which is different for each formation. In order to simplify the results for these shapes and provide a more general expression for R than Equation (10), the following values for r are established for $n=2$, $n=3$ (equilateral triangle), $n=4$ (square) [2]:

$$\begin{aligned} r &= \frac{d}{2}, n = 2 \\ r &= \frac{d}{\sqrt{3}}, n = 3 \\ r &= \frac{d}{\sqrt{2}}, n = 4 \end{aligned} \quad (11)$$

ii. TWO NODES

For the system consisting of $n=2$ nodes and the use of the Pythagorean theorem, the ranges R_R, R_T can be expressed as [2]:

$$R_R^2 = (R^2 + d^2 / 4) - R d \cos \theta \quad (12)$$

$$R_T^2 = (R^2 + d^2 / 4) + R d \cos \theta \quad (13)$$

The product of the above ranges is [2]:

$$R_T R_R = \kappa = \sqrt{R^4 + \frac{R^2 d^2}{2} + \frac{d^4}{16} - R^2 d^2 \cos^2 \theta} \quad (14)$$

For $\kappa = 0$ the above equation transforms to [2]:

$$R^2 = \left(\frac{d}{2}\right)^2 \left[\cos 2\theta + \sqrt{\cos^2(2\theta) + \left(\frac{2\sqrt{k}}{d}\right)^4} - 1 \right] \quad (15)$$

For $n = 2$, we also have [2,4]:

$$r = d/2$$

$$a = \left(\frac{2\sqrt{k}}{d}\right)^4 = \left(\frac{\sqrt{k}}{r}\right)^4 \quad (16)$$

where d is the separation of the sensor nodes.

There are three cases for the Cassini ovals where:

- For $d > 2\sqrt{k}$ we get two ovals centered on each node
- For $d < 2\sqrt{k}$ we get a closed curve
- For $d = 2\sqrt{k}$ the curve is sinusoidal spiral or lemniscates

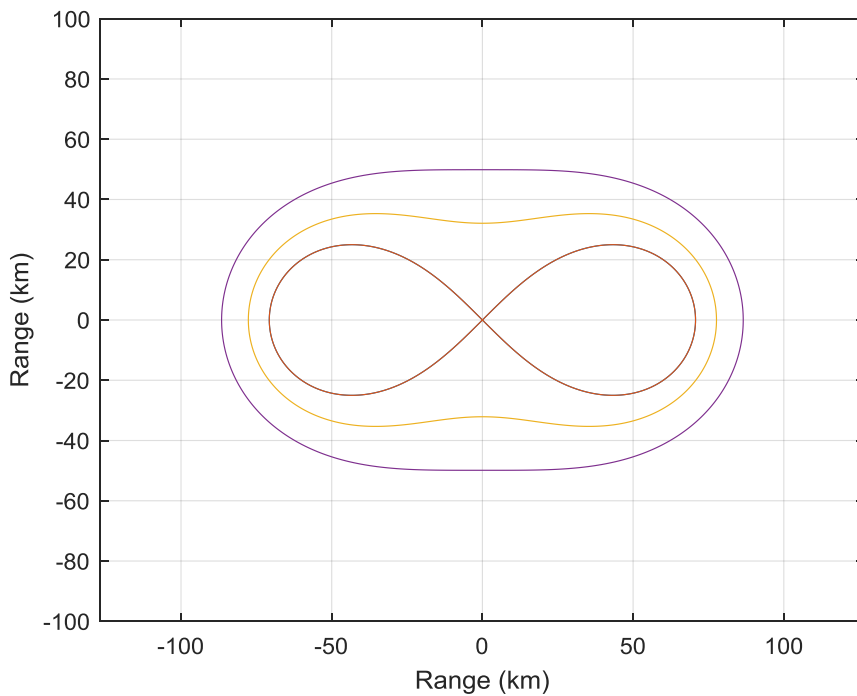


Figure 2. Cassini Ovals for $n = 2$ nodes

iii. THREE NODES

For $n = 3$ nodes configuration we use the same technique as we used for the $n=2$ nodes configuration with [2]:

$$r = d / \sqrt{3}$$

$$a = \left(\frac{\sqrt{\kappa}}{r} \right)^4 = \left(\frac{\sqrt{3}\sqrt{\kappa}}{d} \right)^4 = \frac{9\kappa^2}{d^4} \quad (17)$$

and the three cases for Cassini curves become:

- For $d > \sqrt{3k}$ we get three ovals centered on each node
- For $d < \sqrt{3k}$ we get a closed curve
- For $d = \sqrt{3k}$ the curve is sinusoidal spiral or lemniscate

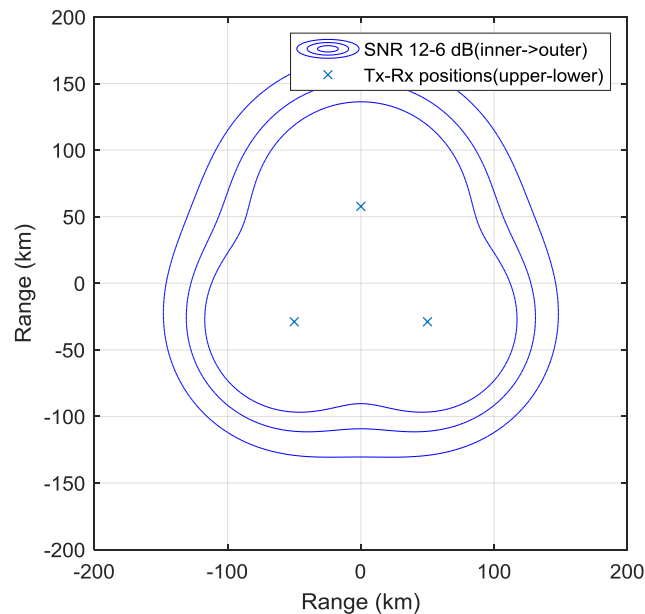


Figure 3. Cassini Ovals for $n=3$ nodes

We observe that the coverage is not symmetrical due to the odd number of nodes. Below we compare the monostatic and a 3-node netted radar network. The extra coverage, due to this configuration, is more than obvious, covering a 360 degrees sector and extending the range even 100 kilometers longer than the monostatic case.

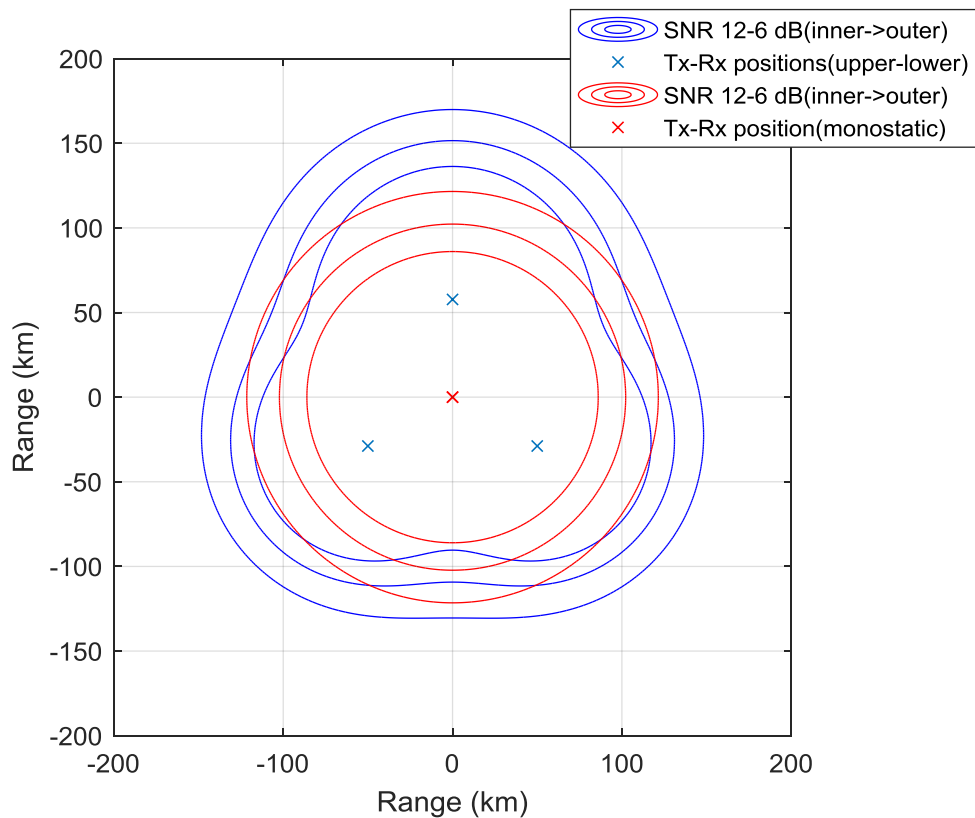


Figure 4. Comparison of coverage between $n = 1$ and $n = 3$ nodes Cassini Ovals

4. LPI RADARS

Radars, in general, transmit pulses with small pulsewidth. This has nothing in common with the LPI radars, where longer duration pulses are emitted in order to deceive the target's systems and believed to be a CW radar emission. This property is expressed by the parameter known as the Duty Cycle of the radar and which expresses the ratio of average power to the maximum radiated power of the radar.

$$dc = P_{avg} / P_{max} \quad (18)$$

LPI radars use waveforms that don't differ from the classical pulse compression waveforms used in conventional pulse doppler radars. The main difference though, is that the signal carrier is a continuous wave. The pulse compression techniques instead, are the same and use frequency coding (frequency shift, FSK) or phase coding (phase shifting, PSK) or combined frequency and phase coding (FSK / PSK waveforms). The extraction of the pulse characteristics from the receiver depend on the complexity of the waveform.

5. AMBIGUITY FUNCTION, PERIODIC AMBIGUITY FUNCTION AND PERIODIC AUTOCORRELATION FUNCTION IN LPI SIGNALS [4]

If we consider a phase-modulated CW signal, where N_c is the number of phase states (codes), while t_b is the duration of each different state (subcode), the period of the signal is given by the relation:

$$T = N_c t_b \quad (19)$$

Then the complex periodic signal is mathematically described by the relationship:

$$u(t) = u(t+nT) = u(t+N_c t_b) \quad (20)$$

where: $n = 0, \pm 1, \pm 2, \pm 3, \dots$

The Autocorrelation Function (ACF) of the signal expresses the response of the tuned filter of the receiver to the input signal. In particular, the response of the filter equals the complex conjugate of the emitted signal. Thus, the input signal passing through the tuned filter, in practice, correlates with its image from which the delay is calculated. The Periodic Autocorrelation Function (PACF) is used on the CW radar and essentially gives exactly what the ACF, the response of the tuned filter to the input signal. The PACF form, however, is different from that of ACF, since the transmitted signal - like the one received - on an LPI radar is a periodic waveform, which contains the NN copy number of the encoded signal. Consequently, the PACF study is more appropriate in the case of LPI radar. The PACF is given by the following relationship:

$$R(\tau t_b) = \frac{1}{N_c} \sum_{n=1}^{N_c} u(n) u^*(n+\tau) \quad (21)$$

Where: τ is the time delay while the operator (*) denotes the complex conjugate. Given that the signal is continuous and periodic, it follows from the above equation that the PACF is maximal when the delay takes values that are multiples of the code period t_b , ie:

$$R(\tau t_b) = \begin{cases} 1, & \tau = 0(\text{mod}N_c) \\ 0, & \tau \neq 0(\text{mod}N_c) \end{cases} \quad (22)$$

Equation (22) practically means that CW waveforms, formed by a periodic function, can theoretically have the ideal PACF, i.e. zero side lobes. The autocorrelation function is sufficient to describe whether the received radar signal is shifted in time relative to its emitted analog, but it does not give any information about the change in its doppler frequency. As known, when the signal returning to the receiver is derived from a moving target, it has a frequency shift due to

doppler the size of which needs to be known so that the frequency response of the tuned receiver is suitably matched to the frequency of the received signal, so it finally operates the tuned filter correctly.

Thus, the Periodic Ambiguity Function (PAF) is defined as the function describing the result of the correlation of N periodic copies of the emitted signal to the received CW signal for target detection. In fact, PAF expresses the response of the matched radar receiver to the input signal and includes any change in the doppler frequency and also in the delay. PAF is the analog of the Ambiguity Function (AF) used in pulse radars. The only difference is that PAF refers to a continuous wave radar where the transmitted CW signal is formed by a periodic function with period T , whereby the reference signal for the tuned receiver is a signal consisting of N periods. So if $u(t)$ is the reference signal generated by N number of periods, then PAF for the tuned receiver is given by:

$$|\chi_{NT}(\tau, \nu)| = \left| \frac{1}{NT} \int_0^{NT} u(t-t)u^*(t)e^{j2\pi\nu t} dt \right| \quad (23)$$

where the delay τ is considered constant, while ν is the doppler displacement. It can also be shown that the following relationship applies:

$$|\chi_{NT}(\tau, \nu)| = |\chi(\tau, \nu)| \left| \frac{\sin(N\pi\nu T)}{N \sin(\pi\nu T)} \right| \quad (24)$$

where: $|\chi(\tau, \nu)|$ is the PAF for a period of the signal. Consequently, PAF of N signal periods can be calculated by multiplying the PAF of a period as in equation (23). It should be noted that the corresponding PACF of N periods of a signal result from the PACF of a period multiplied simply by N .

Similarly to AF, PAF has a maximum equal to 1 when $\nu = \tau = 0$ (beginning of axes) in the sense that the response of the custom filter is always the maximum when the associated signal is the copy of itself when is not delayed in time or altered in frequency. So by studying PAF, we can see changes in the frequency or time of the received signal. PAF also shows symmetry wrt both axes (ν, τ). In terms of time, the symmetry of PAF is expressed by the relationship:

$$|\chi_{NT}(nT, \nu)| = |\chi_{NT}(0, \nu)| \quad (25)$$

where: n is any integer. Similarly, in terms of Doppler frequency, symmetry is expressed as:

$$|\chi_{NT}(\tau, m/T)| = |\chi_{NT}(\tau + \nu T, m/T)| \quad (26)$$

where: m/T are intersections along the doppler axis ($\nu = m/T$) and $m = 0, \pm 1, \pm 2, \dots$

It is easy to see that for $\nu = 0$, which is equivalent to the intersection of the time axis, the PAF graph is the same as the PACF.

i. Pulse

To begin with we will start observing the Ambiguity Function (AF) and Periodic Ambiguity Function (PAF) of a constant frequency pulse (unmodulated) in order to start as simple as possible.

The Ambiguity Function of this pulse is illustrated below [5]:

$$\chi(\tau, \nu) = \int_{-\infty}^{\infty} u(t) u^*(t + \tau) \exp(j2\pi\nu t) dt \quad (27)$$

In Figure 5, in which the two quadrants of the pulse are plotted, the triangular zero Doppler cut is shown clearly. The pulse's parameters, autocorrelation and spectrum plots are also shown below along with the Periodic Ambiguity plot.

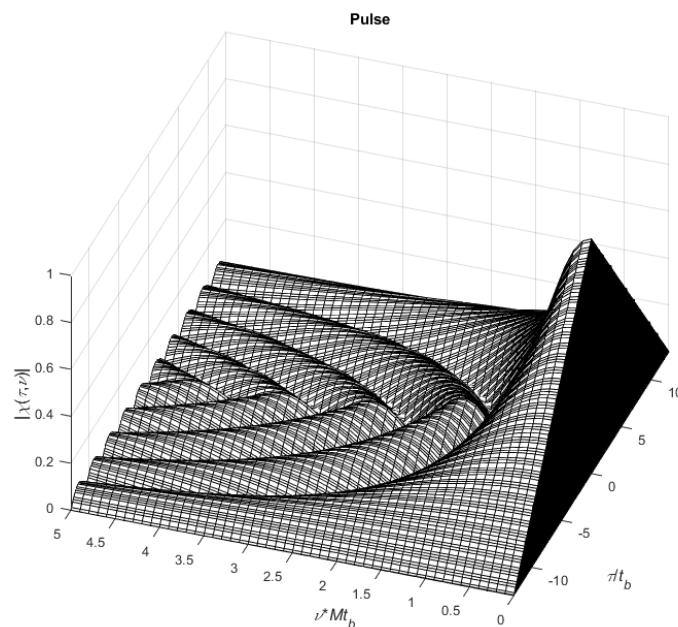


Figure 5. Ambiguity function plot of a constant frequency pulse

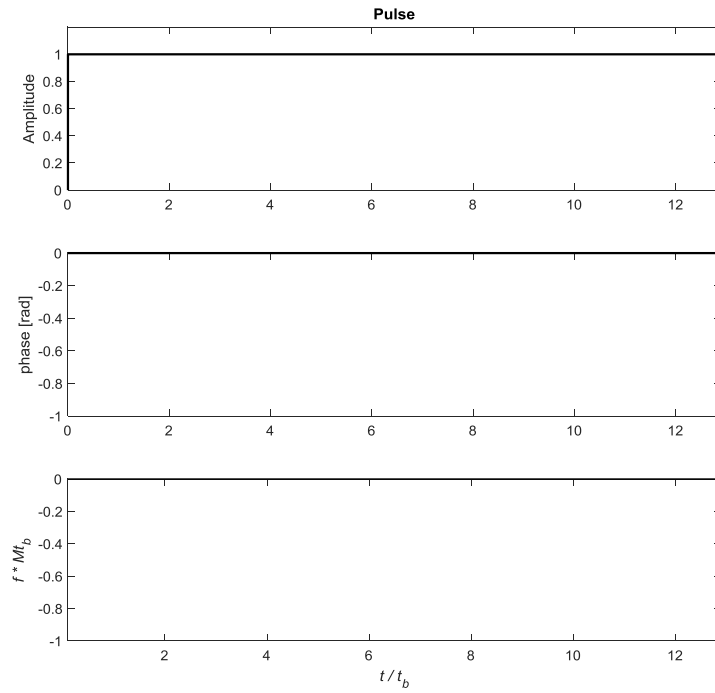


Figure 6. Signal parameters plot of a constant frequency pulse

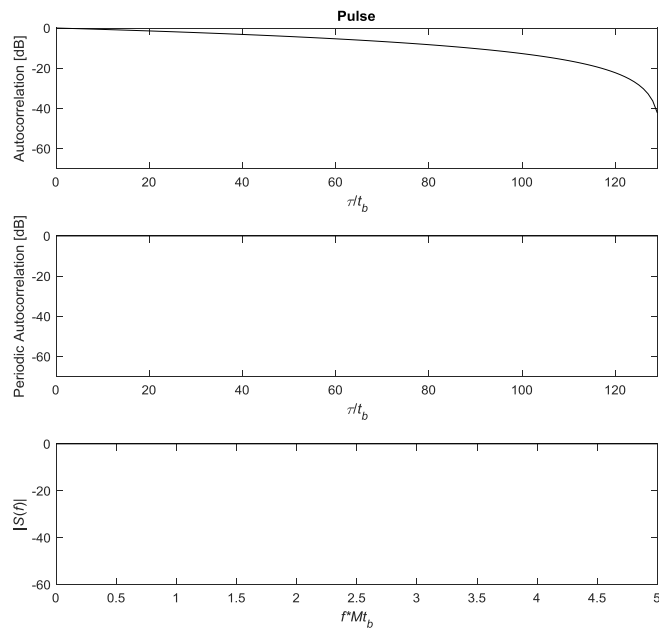


Figure 7. Autocorrelation and Spectrum plots of a constant frequency pulse

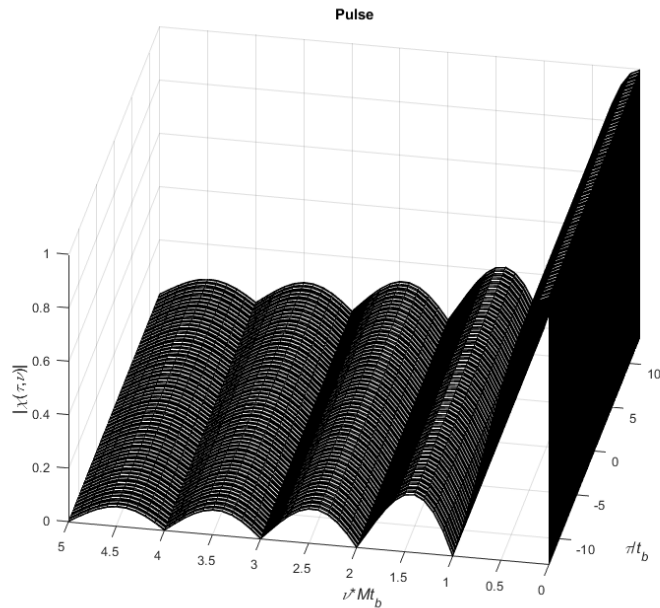


Figure 8. Periodic Ambiguity function plot of a constant frequency pulse

If more than one unmodulated pulses are transmitted, we are talking about a coherent pulse train (CPT). In our Ambiguity Function, signal characteristics, autocorrelation and Spectrum and Periodic Ambiguity Function plots we use six identical pulses. The production of more complicated signals though, needs some diversity.

ii. Coherent Pulse Train

For a coherent pulse train the Ambiguity Function is [5] :

$$|\chi(\tau, \nu)| = \frac{1}{N} \sum_{p=-(N-1)}^{N-1} |\chi_T(\tau - pT_r, \nu)| \left| \frac{\sin[\pi\nu(N-|p|)T_r]}{\sin \pi\nu T_r} \right|, \quad \begin{array}{l} |\tau| \leq NT_r \\ |\tau| \leq T \end{array}, \text{ zero elsewhere} \quad (28)$$

where $|\chi_T(\tau, \nu)|$ is Ambiguity Function of an individual pulse. For the illustrated unmodulated pulse below, we use the equation [5] :

$$|\chi_T(\tau, \nu)| = \left| \left(1 - \frac{|\tau|}{T} \right) \frac{\sin[\pi T \nu (1 - |\tau|/T)]}{\pi T \nu (1 - |\tau|/T)} \right|, \quad |\tau| \leq T, \text{ zero elsewhere} \quad (29)$$

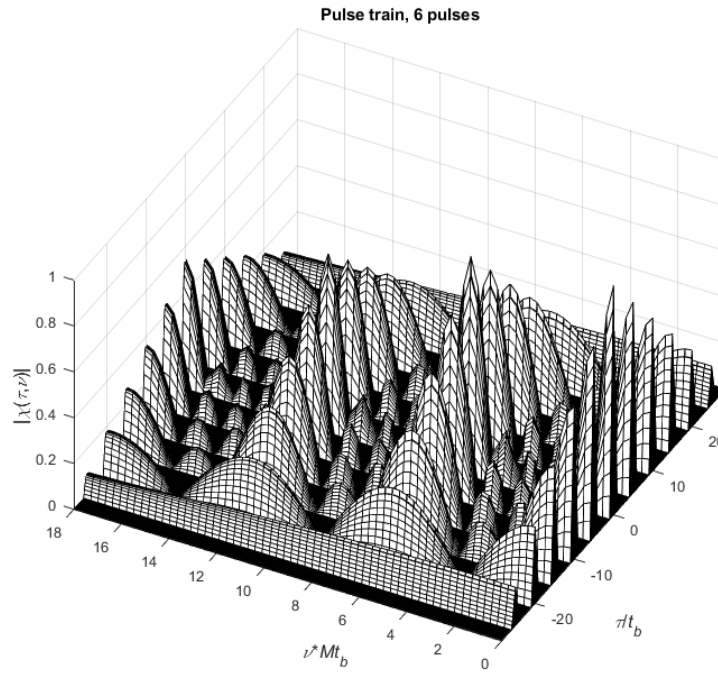


Figure 9. Ambiguity function plot of a 6 pulses Pulse train

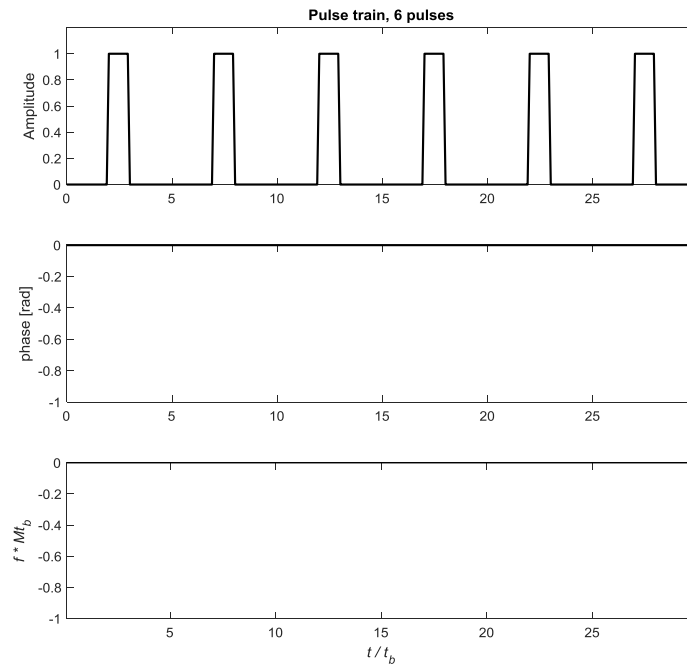


Figure 10. Signal parameters plot of a 6 pulses Pulse train

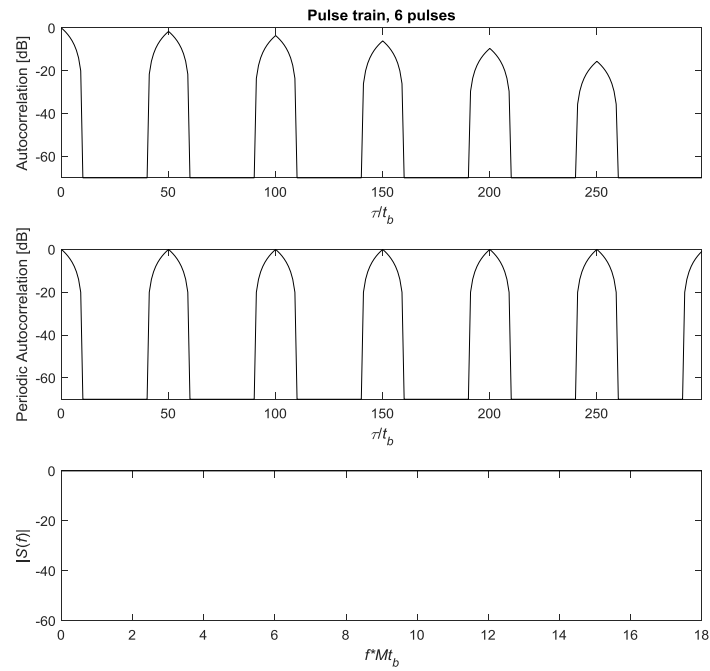


Figure 11. Autocorrelation and Spectrum plots of a 6 pulses Pulse train

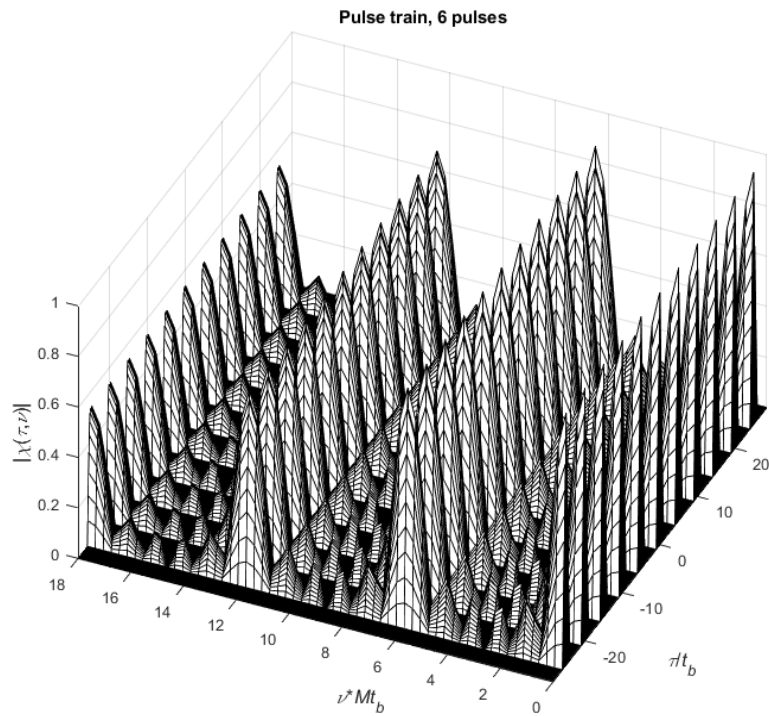


Figure 12. Periodic Ambiguity function plot of a 6 pulses Pulse train

iii. Linear Frequency Modulated (LFM) and Weighted Linear Frequency Modulated (LFM) CW signal

If pulse compression method has to be introduced in order to have more efficient along with complicated pulses, then we should start with the frequency modulation method. The well-known Linear Frequency Modulation (LFM) is the one that will be discussed first. Its Ambiguity Function is [5]:

$$|\chi(\tau, \nu)| = \left| \left(1 - \frac{|\tau|}{T}\right) \frac{\sin(\pi T(\nu \mp B(\tau/T))(1 - |\tau|/T))}{\pi T(\nu \mp B(\tau/T))(1 - |\tau|/T)} \right|, \quad |\tau| \leq T, \text{ zero elsewhere} \quad (30)$$

Figure 14 illustrates the phase and frequency variation of a Linear Frequency Modulated (LFM) CW signals. Figure 16 shows the PAF of the signal while in Figure 15 is shown its corresponding ACF and PACF. M is the number of signal samples, while t_b is the sampling time, so obviously the total duration of the signal is Mt_b . One of the desired characteristics of the PAF of an LPI waveform is that the level of the side lobes must be as minimal as possible. This is because when the return of a target from the radar sidelobes is strong, there is the possibility that a smaller RCS target will not be detected because its return is lost in the sidelobes of the previous target.

The FMCW radar originally was designed to address the weakness of CW radar (unmodulated signal) to calculate the distance of a target. Afterwards, it turned out that FMCW waveforms have very good LPI features and also have several interesting advantages. FMCW waveforms have increased interference resistance in the sense that they are deterministic signals, and consequently any interfering signal lacking the same mathematical pattern can be recognized by the radar receiver and discarded, [2]. Yet another advantage is that the energy of the emitted signal diffuses over a wide modulation bandwidth, resulting in the signal eventually being very low in power and therefore difficult to detect. This is particularly desirable in cases where a low level of emissions from a platform is required. Figure 15 shows the ACF and PACF of the signal. As shown, the level of the side lobes in the ACF is relatively low, but the signal does not have the ideal PACF since there are sidelobes over time in the PACF plot. Figure 16 also shows the PAF of the signal, where the side lobes are plotted in terms of the doppler frequency, meaning that the signal does not behave well in the presence of doppler shifts.

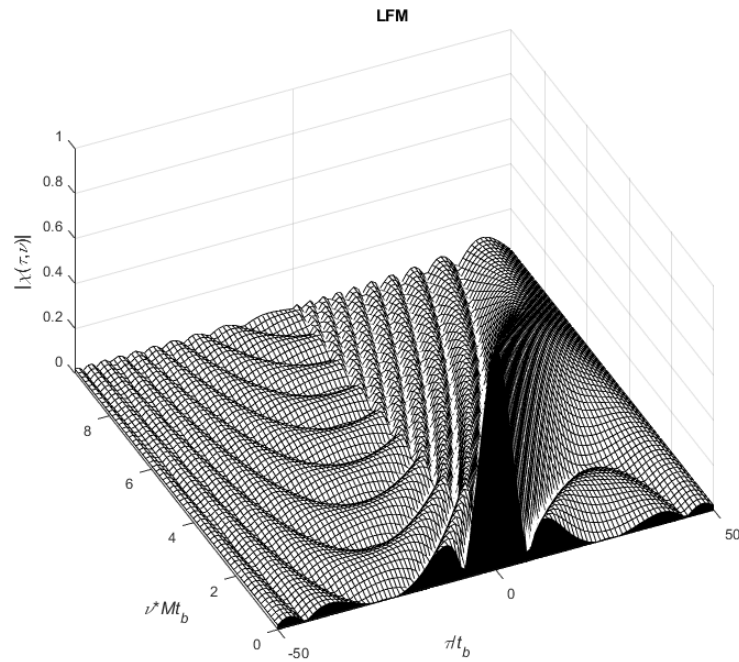


Figure 13. Ambiguity Function plot of a Linear Frequency Modulated (LFM) CW signal

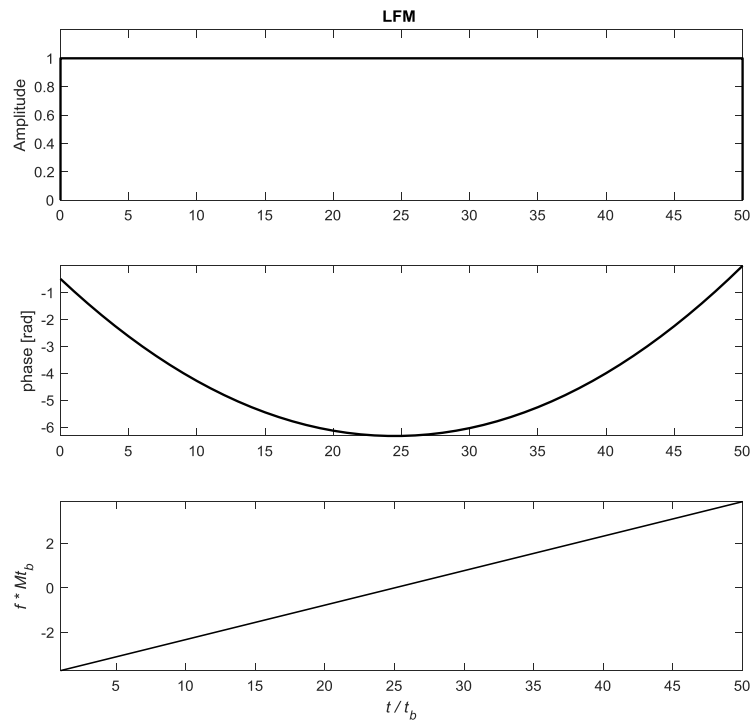


Figure14. Signal parameters plot of a Linear Frequency Modulated (LFM) CW signal

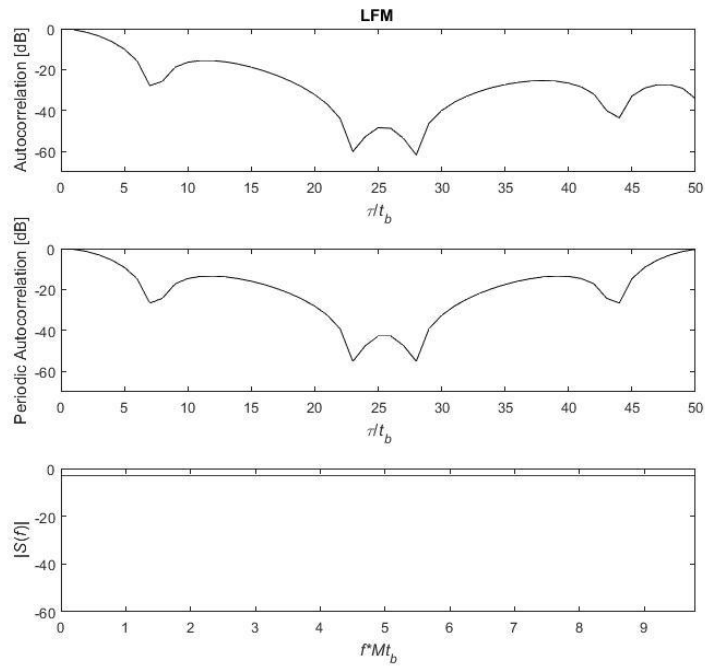


Figure 15. Autocorrelation and Spectrum plot of a Linear Frequency Modulated (LFM) CW signal

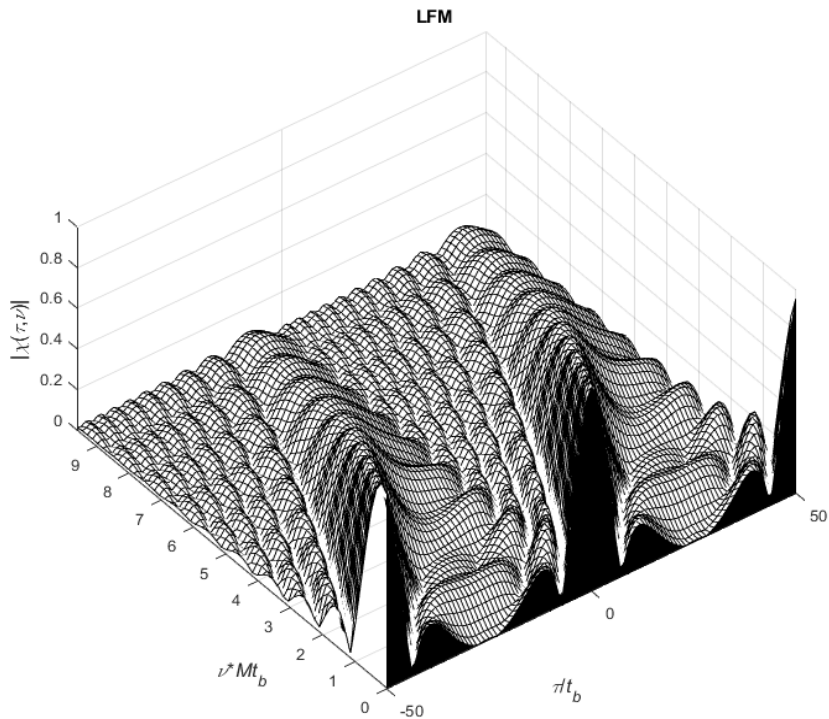


Figure 16. Periodic Ambiguity function of a Linear Frequency Modulated (LFM) CW signal

LFM has the positive outcome of improved range resolution, resulting from the increase of the bandwidth. The negative outcome of the LFM signal is the sidelobes' amplitude, that can be observed in Figure 13. In order to mitigate this phenomenon, spectral reshaping with amplitude or frequency weighting was introduced. In this simulation, the Hamming weighted LFM pulse was used.

Comparing Figure 13 with Figure 17 it is obvious that the sidelobes of the central lobe are reduced. It has also been observed the weighting has effects even at higher Doppler frequencies.

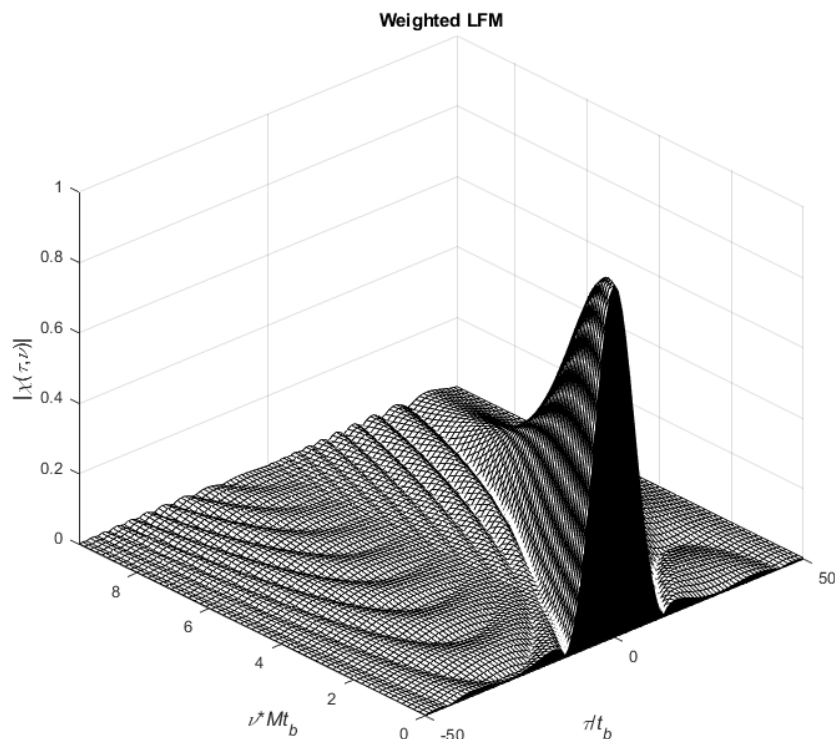


Figure 17. Ambiguity function plot of a weighted LFM signal

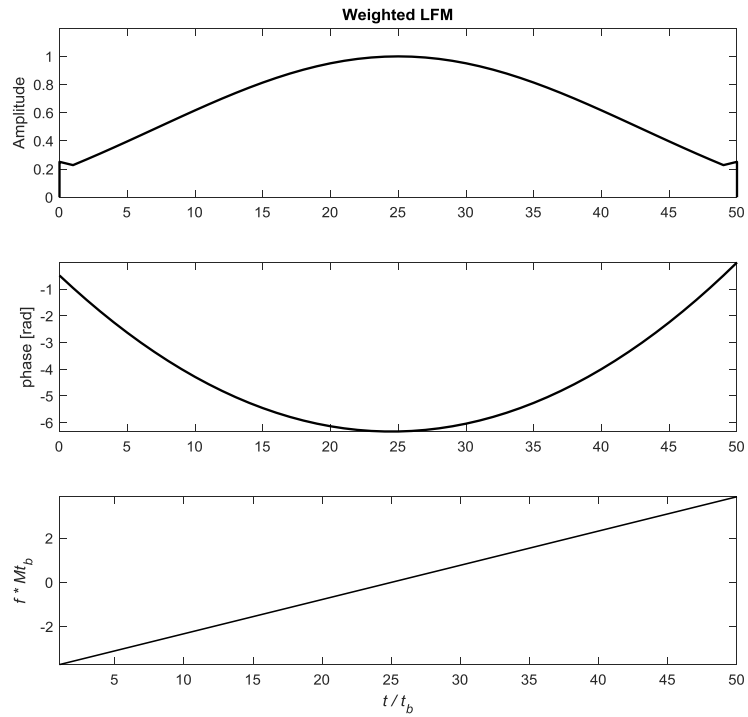


Figure 18. Signal parameters plot of a weighted LFM signal

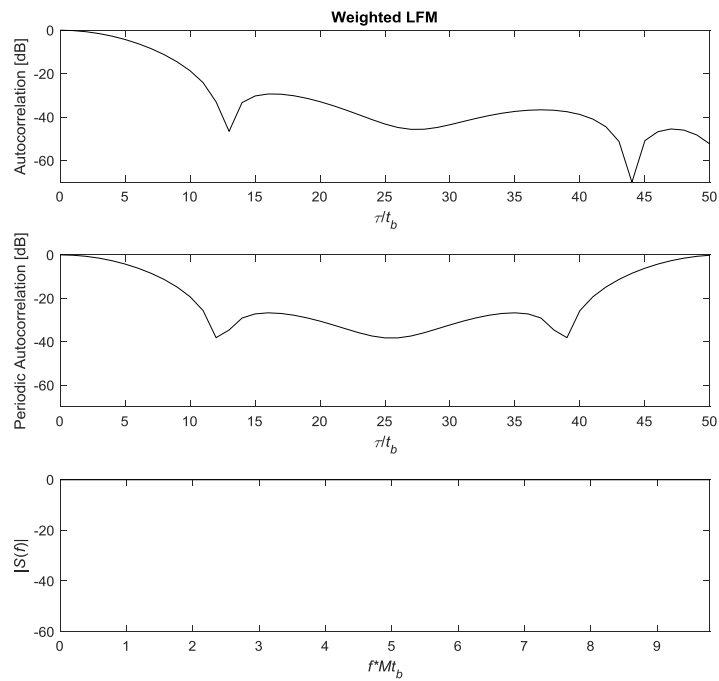


Figure 19. Autocorrelation and Spectrum plots of a weighted LFM signal

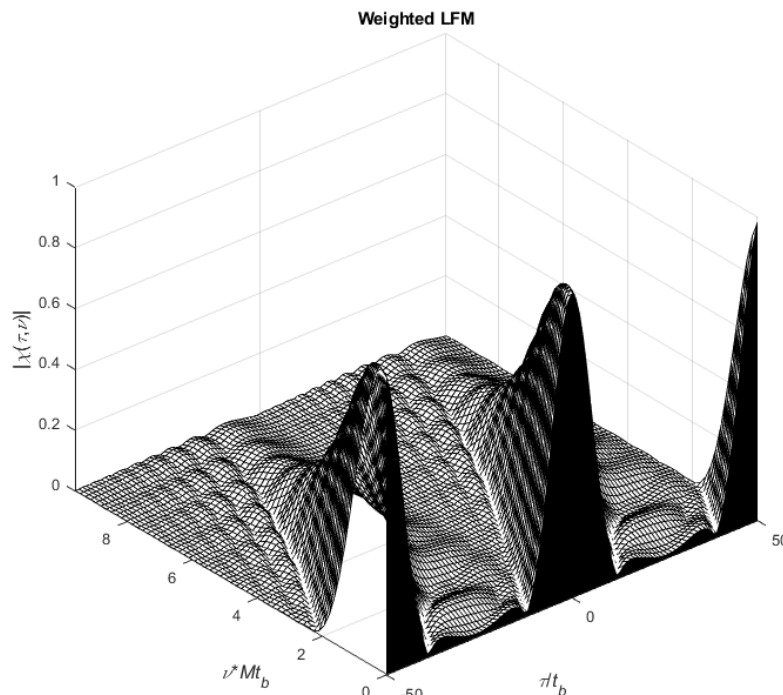


Figure 20. Periodic Ambiguity function plot of a weighted LFM signal

iv. Costas code

Another technique that is named Costas, is the exact opposite LFM pulses. It uses discrete frequency coding .

The Autocorrelation function of Costas can be found by overlapping two same matrices and in turn shifting them, in order to take into account delay (horizontal axis shifts) and Doppler (vertical axis shifts).

In the LFM, the number of coinciding dots will be $N = M - |m|$, representing delay and Doppler shifts of equal number of units. In the Costas signal case, this number's maximum value is one for all but the zero-shift case, where all dots coincide ($N = M$).

This unique characteristic gives us a narrow peak of the Ambiguity Function at the origin, and low sidelobes anywhere else.

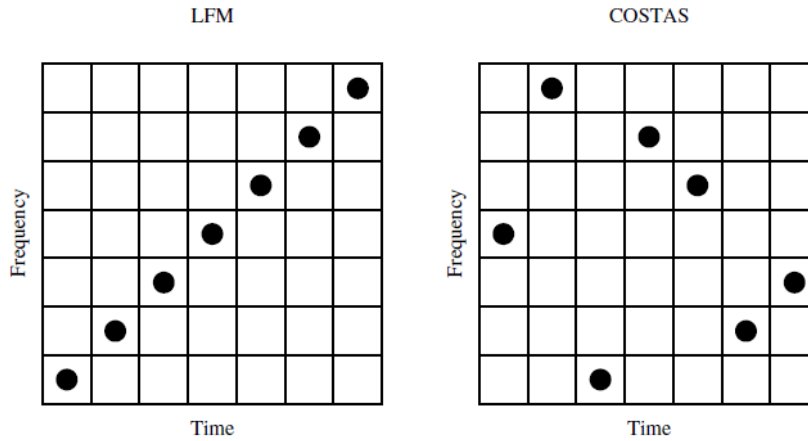


Figure 21. Binary matrix representation of LFM (left) and Costas coding (right) [5]

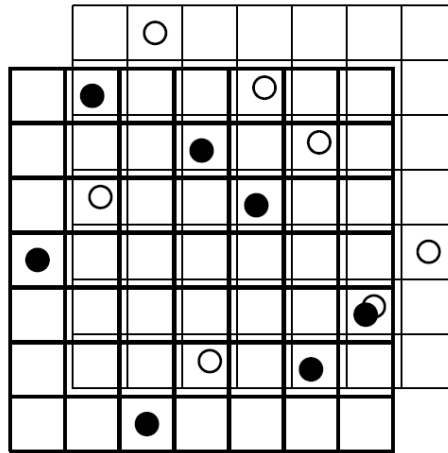


Figure 22. Example of one coincidence occurring at $\tau/\tau_b=1, \nu/\Delta f=1$ [5]

A closed-form expression of the Ambiguity Function of Costas is [5]:

$$\chi(\tau, \nu) = \frac{1}{M} \sum_{m=1}^M \exp[j2\pi(m-1)\nu t_b] \{ \Phi_{mm}(\tau, \nu) + \sum_{\substack{n=1 \\ m \neq n}}^M \Phi_{mn}[\tau - (m-n)t_b, \nu] \} \quad (31)$$

where $\Phi_{mn}(\tau, \nu) = \left(1 - \frac{|\tau|}{t_b}\right) \frac{\sin \alpha}{a} \exp(-j\beta - 2j2\pi f_n \tau), \quad |\tau| \leq t_b, \text{ zero elsewhere,} \quad (32)$

in which $\alpha = \pi(f_m - f_n - \nu)(t_b - |\tau|) \quad , \quad \beta = \pi(f_m - f_n - \nu)(t_b + \tau) \quad (33)$

Below are plotted the Ambiguity Function (AF) (Fig. 23), the Autocorrelation Function (ACF) and Periodic Autocorrelation Function (PACF) (Fig. 25) and the Periodic Ambiguity Function (PAF) (Fig. 26) plots of the Costas signal derived from the numerical Ambiguity Function plotting program. The Ambiguity Function is calculated from coherent processing and the

sidelobe matrix doesn't use phase coherence. From these indications we proceed to the result that non-coherent processing will fit to Costas signals. At the zero-Doppler cut are shown various zero values at multiples of t_b and there are many sidelobes, as expected.

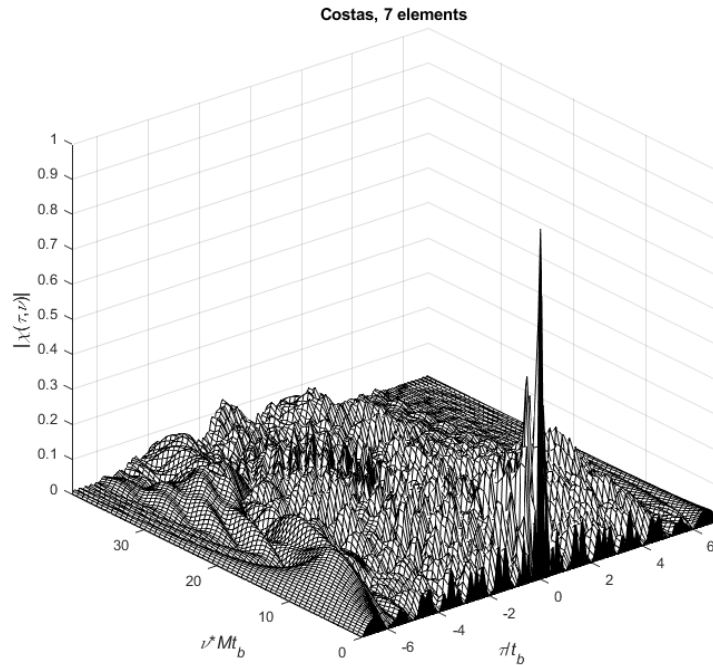


Figure 23. Ambiguity function plot of a 7 elements Costas signal

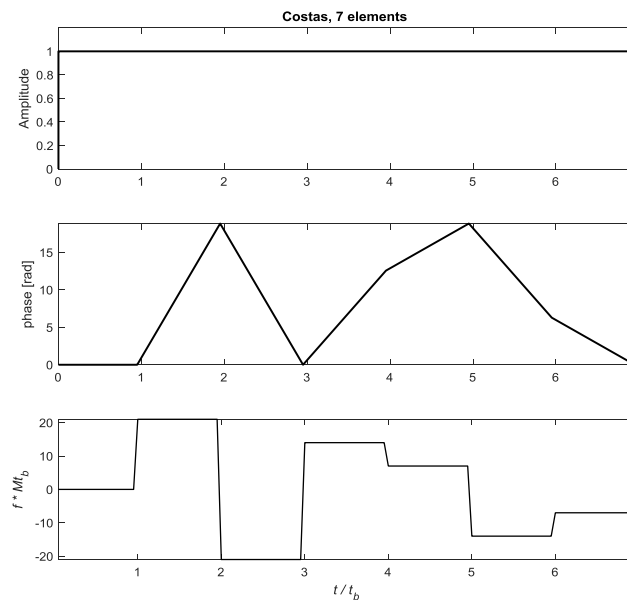


Figure 24. Costas signal parameters plot of a 7 elements Costas signal

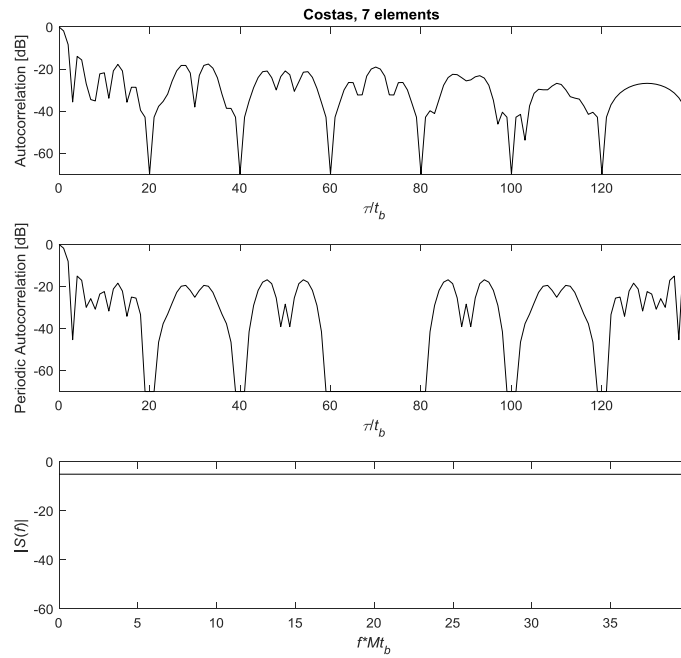


Figure 25. Autocorrelation and Spectrum plot of a 7 elements Costas signal

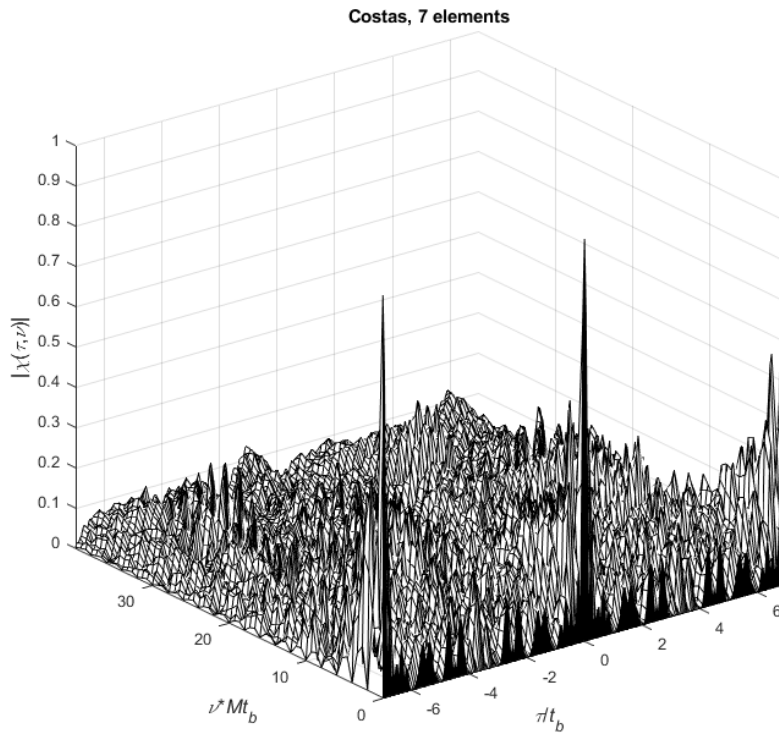


Figure 26. Periodic Ambiguity Function (PAF) of a 7 elements Costas signal

v. Barker code

Another pulse, that uses phase coding is named Barker code signal. It uses a set of M binary phases generating a peak-to-peak sidelobe ratio of M . It is well known that no binary Barker codes exists for $13 < M < 1$ and for all odd $M > 13$. It is also widely believed that there is no Barker code for all $M > 13$. The main positive aspect of the binary Barker is its simplicity. Its main drawback is its limitation concerning the values of M . Below there is a table of all known binary Barker Codes followed by the Autocorrelation Function, Signal parameters, Autocorrelation and Spectrum and the Periodic Autocorrelation function plots.

Code Length	Code
2	11 or 10
3	110
4	1110 or 1101
5	11101
7	1110010
11	11100010010
13	1111100110101

Table 2. Binary Barker codes

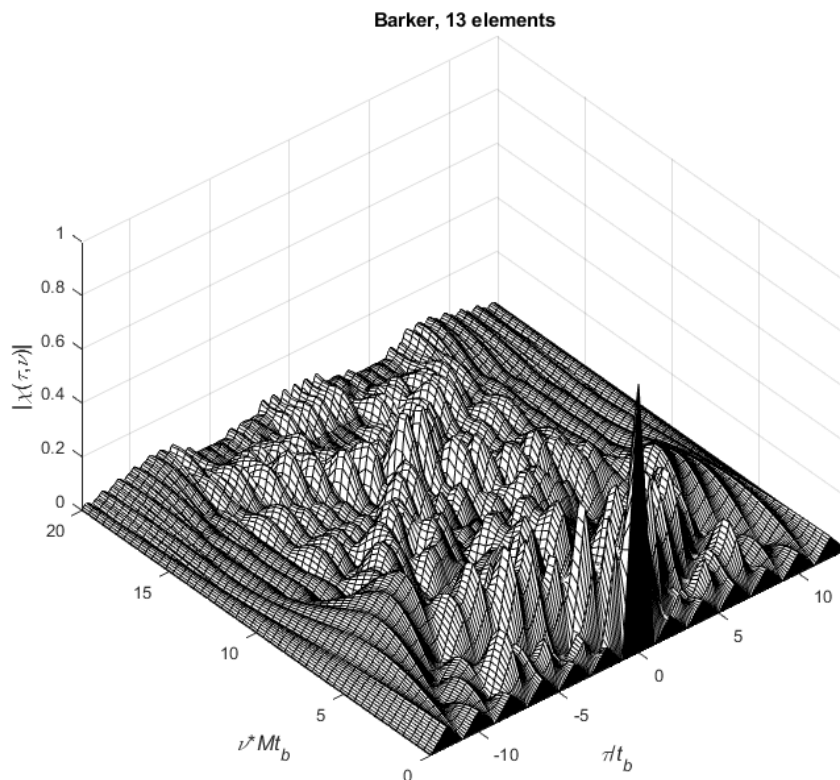


Figure 27. Ambiguity function plot of a 13 elements Barker code signal

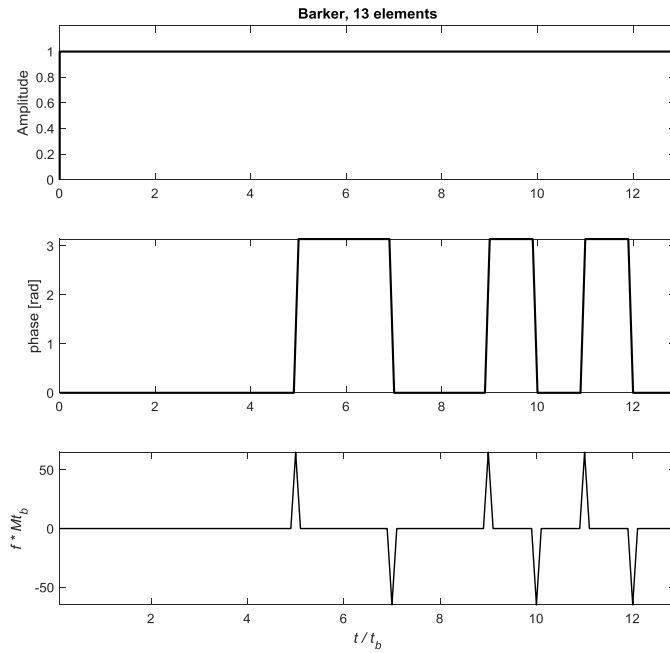


Figure 28. Signal parameters plot of a 13 elements Barker code signal

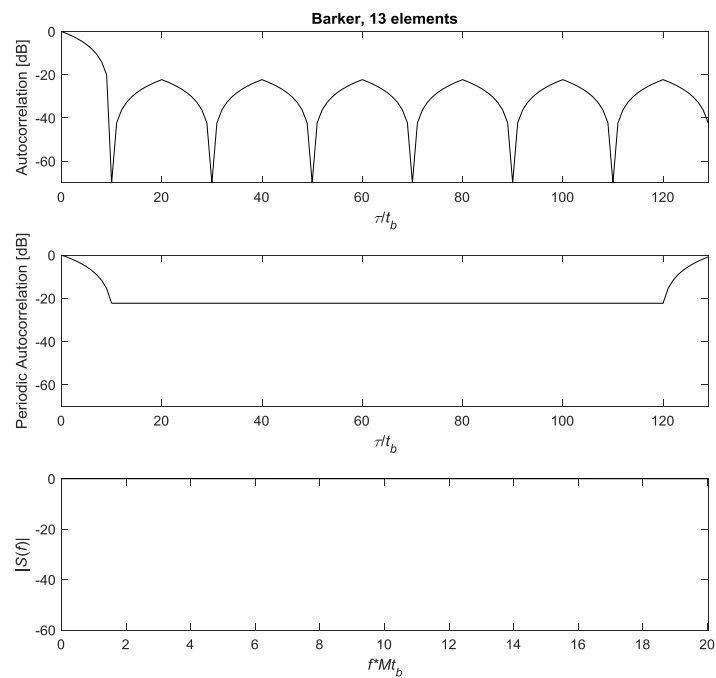


Figure 29. Autocorrelation and Spectrum plots of a 13 elements Barker code signal

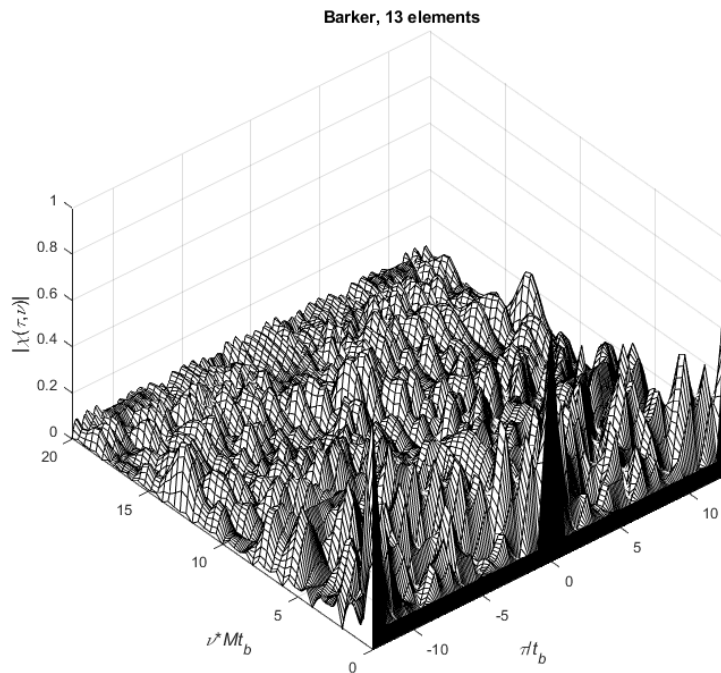


Figure 30. Periodic Ambiguity function plot of a 13 elements Barker code signal

vi. Frank code PSK

Frank code PSK waveforms are widely used in LPI radars, implementing the linear frequency modulation stepwise (step approximation). The values of the code were expressed by Frank using the elements of an $L \times L$ discrete Fourier transform matrix given by [5]:

$$\begin{bmatrix} 0 & 0 & 0 & \cdots & 0 \\ 0 & 1 & 2 & \cdots & L-1 \\ 0 & 1 & 4 & \cdots & 2(L-1) \\ \vdots & \vdots & \vdots & \ddots & \vdots \\ 0 & L-1 & 2(L-1) & \cdots & (L-1)^2 \end{bmatrix} \quad (34)$$

The original Frank code has two important properties:

- i) the code is perfect and
- ii) the aperiodic autocorrelation exhibits relatively low sidelobes

Its main negative property is that it is applied only for codes of perfect square length ($M = L^2$).

The Ambiguity Function (AF) of a 16-element Frank Code signal is plotted below (Figure 32) along with its Autocorrelation Function (ACF) , the Periodic Autocorrelation Function (PACF) (Figure 34) and its Periodic Ambiguity Function (PAF) (Figure 35).

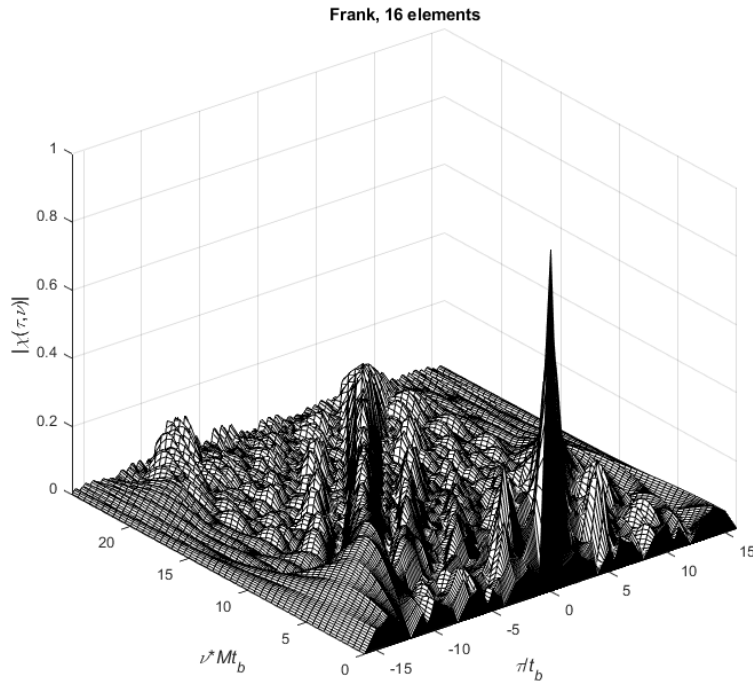


Figure 31. Ambiguity function plot of a 16 elements Frank Code signal

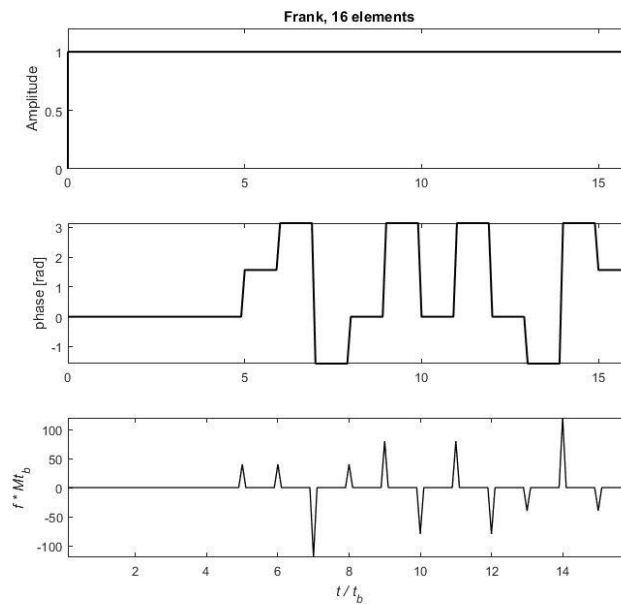


Figure 32. 16 Signal parameters plot of a 16 elements Frank Code signal

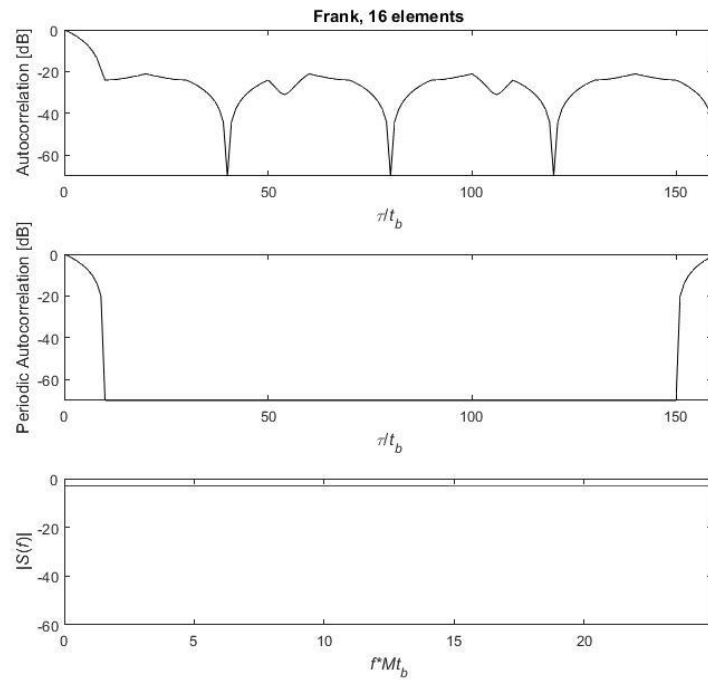


Figure 33. Autocorrelation and Spectrum plots of a 16 elements Frank Code signal

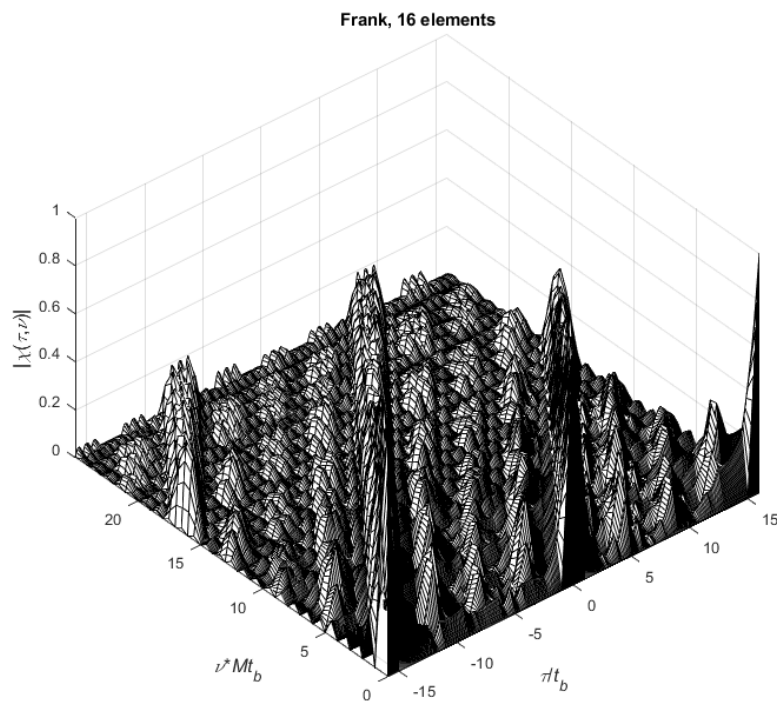


Figure 34. Periodic Ambiguity function plot of a 16 elements Frank Code signal

vii. Polyphase codes P1, P2, P3, P4

Instead of using Frank code, we can use other PSK waveforms called polyphase codes. Polyphase codes simulate the Linear Frequency Modulation (LFM) waveform. They differ from each other, having different code for the signal phase changes and the way they are generated in hardware. P1, P2, P3 and P4 codes have low level of sidelobes in the ACF and excellent tolerance to Doppler shifts.

P1, P2, P3 and P4 codes were introduced by Lewis and Kretschmer (P1, P2:1981 and P3,P4:1982).

P1 and P2 codes are stem from the Frank code. Their main drawback is that they can be applied only for square length (such as the Frank code). On the other hand, P3 and P4 codes are can be applied for any length M .

Lewis and Kretschmer later on (1983), proved that P3 and P4 codes show more tolerance than the Frank or P1 and P2 codes to Doppler shifts. For this reason we used P4 codes in our plots.

P4 code is defined for any length by [5]:

$$\varphi_m = \frac{2\pi}{M}(m-1)\left(\frac{m-1-M}{2}\right), \text{ where } 1 \leq m \leq M \quad (35)$$

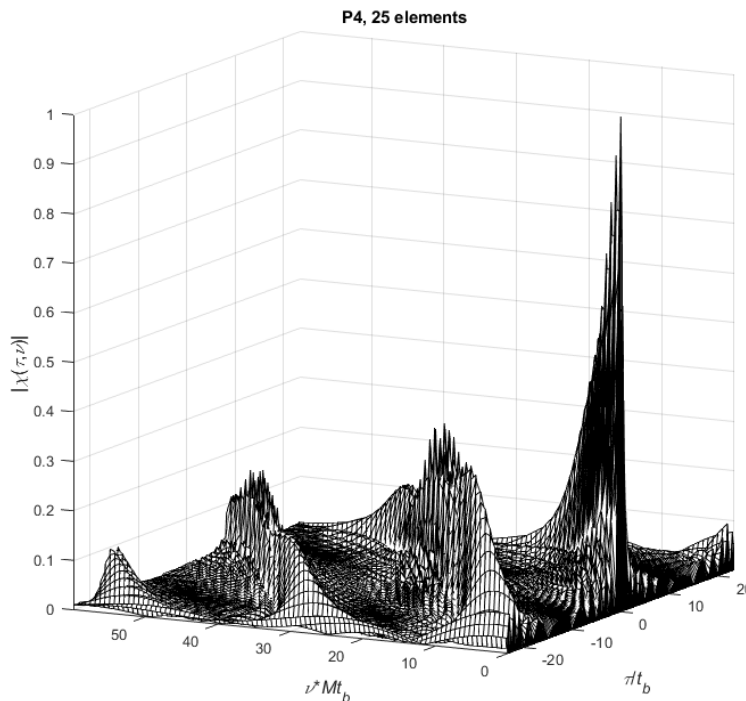


Figure 35. Ambiguity function plot of a 25 elements P4 signal

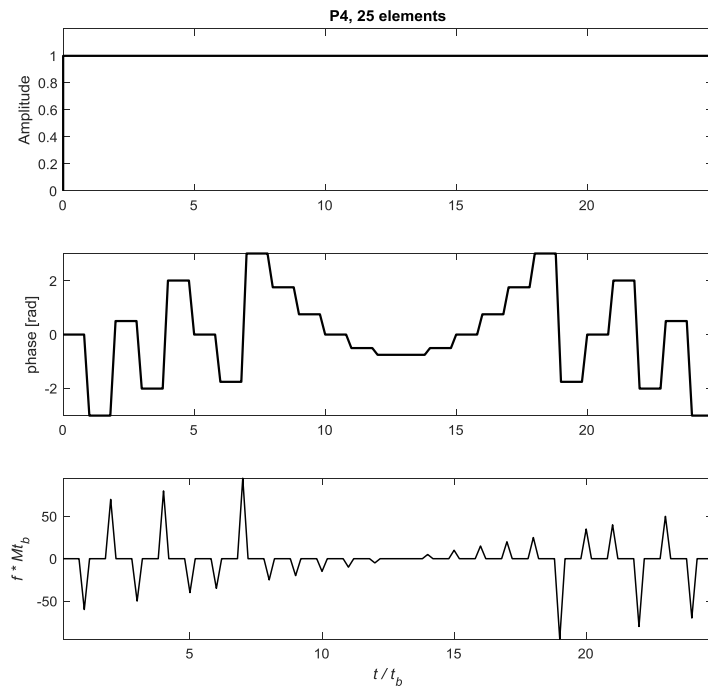


Figure 36. Signal parameters plot of a 25 elements P4 signal

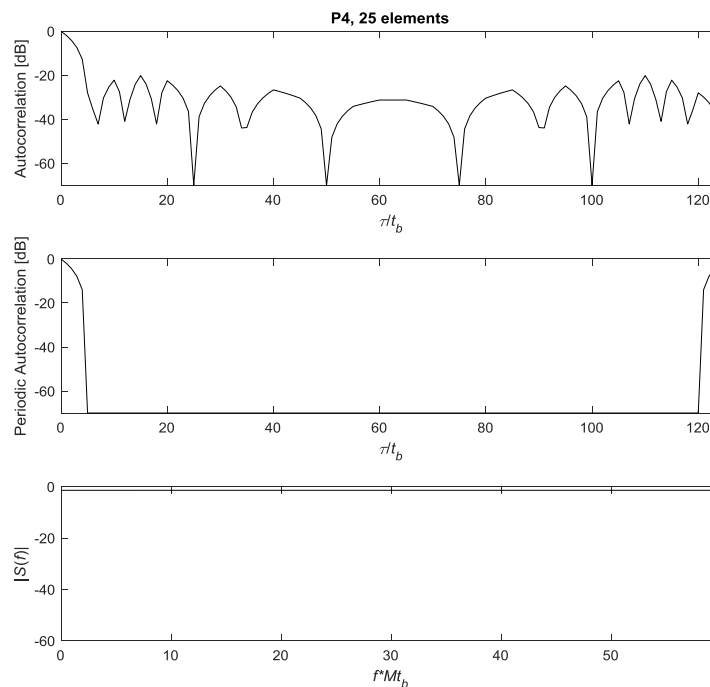


Figure 37. Autocorrelation and Spectrum plots of a 25 elements P4 signal

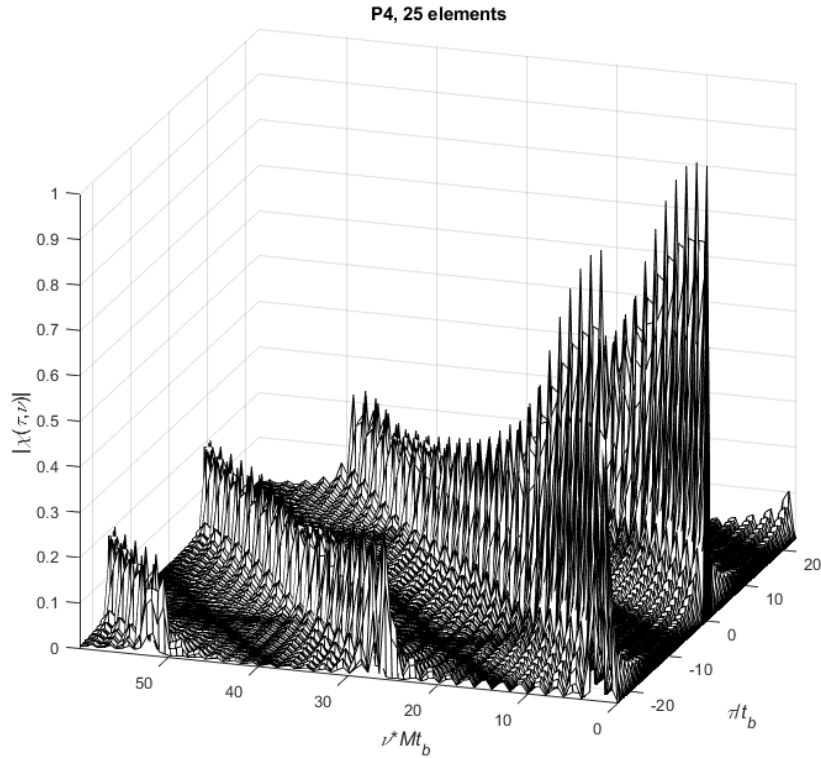


Figure 38. Periodic Ambiguity function plot of a 25 elements P4 signal

6. AMBIGUITY FUNCTION IN A BISTATIC RADAR [3]

The Ambiguity Function of the Monostatic Radar (Equation 1) differs depending on the relative target position in the bistatic plane. The Tsao et. Al. [3] version of this equation shows the non-linear relationships between target velocity and Doppler shift. Also, between target range and delay. The Ambiguity Function for a bistatic radar configuration is expressed as [3]:

$$\left| \chi(R_{R_H}, R_{R_A}, V_H, V_a, \theta_R, L) \right|^2 = \left| \int_{-\infty}^{+\infty} \tilde{f}(t - \tau_a(R_{R_A}, \theta_R, L)) \tilde{f}^*(t - \tau_H(R_{R_H}, \theta_R, L)) \cdot \exp \left[-j \left(\omega_{D_H}(R_{R_H}, V_H, \theta_R, L) - \omega_{D_a}(R_{R_a}, V_a, \theta_R, L) \right) t \right] dt \right|^2 \quad (36)$$

where R_R and R_T are the ranges of the target from the transmitter and the receiver, V is the bistatic range rate, θ_R is the angle of the target measured from the receiver, L is the bistatic baseline, T is the transmitter–target–receiver delay time and subscripts H and a are hypothesized and actual values.

The illustration of this equation is depicted in the figures below, where a target's location and direction gives us the ambiguity function's results for four different cases (Figure 3 a,b,c,d). The waveform used is consisted of three rectangular pulses. From these figures we assume that when the target approaches the baseline between the receiver and the transmitter Figure 3 c,d (in Figure 3d a complete change of the scheme is observed), the change of the plot is more drastical than that of Figure 3 a,b, where the target approaches from a different direction.

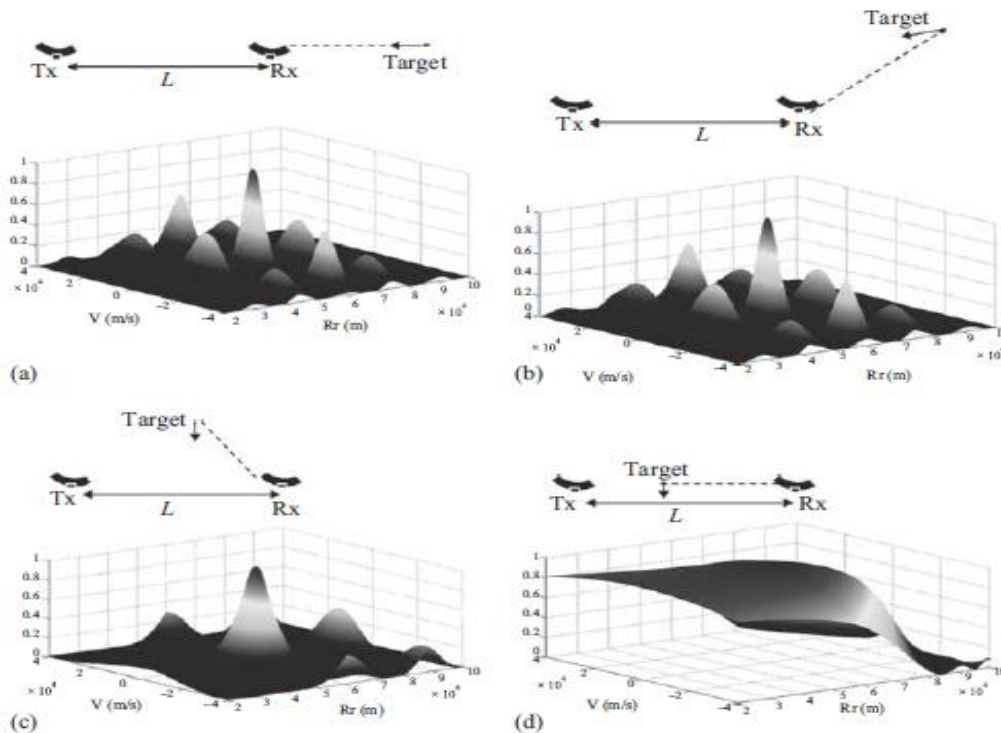


Figure 39. Bistatic ambiguity functions for four different target patterns [1]

7. CONCLUSIONS

As noted, bistatic radar alone cannot provide an adequate correlation peak for all relative locations of the target versus the Tx/Rx pair (e.g Figure 39). Thus, the netted radar solution seems to provide a realistic capability of detecting a target by accumulating individual target detections from the scattered receivers in the net. Regarding the LPI waveforms, P4 coding is a brilliant choice for a modern radar configuration due to low level of sidelobes in the ACF and excellent tolerance to Doppler shifts. Research continues in order to help the derivation of algorithms for optimal detection and the frequency range (e.g. DVB-T, FM) where a netted radar network can provide us a better performance in stealth target detection.

REFERENCES

1. F. Gini et. al. (Eds) (2012), “*Waveform Design and Diversity for Advanced Radar Systems*”, IEE ISBN 978-1-84919-266-8 (PDF).
2. N. Willis, “*Bistatic Radar*”, Scitech Publ, 2005.
3. T. Tsao, et.al. , “*Ambiguity function for a bistatic radar*”, IEEE Trans. Aerosp. Elect. Sys.,vol. 33, no. 3, pp. 1041–1051, July 1997.
4. G. Tsolis, (2011), “*Analysis and Processing of LPI Waveforms using Hilbert- Huang Transform and their Classification with Support Vector Machines*”, PhD Dissertation, Aristotle University of Thessaloniki.
5. Nadav Levanon, Eli Mozeson , “*Radar Signals*, Wiley, 2004.
6. Baker, C. J. and Hume, A. L., “*Netted Radar Sensing*,” Proceedings of the CIE International Radar Conference , pp. 110-114, 2001.